PHYSICS

Fast, noise-free memory for photon synchronization at room temperature

Ran Finkelstein,* Eilon Poem,* Ohad Michel, Ohr Lahad, Ofer Firstenberg†

Future quantum photonic networks require coherent optical memories for synchronizing quantum sources and gates of probabilistic nature. We demonstrate a fast ladder memory (FLAME) mapping the optical field onto the superposition between electronic orbitals of rubidium vapor. Using a ladder-level system of orbital transitions with nearly degenerate frequencies simultaneously enables high bandwidth, low noise, and long memory lifetime. We store and retrieve 1.7-ns-long pulses, containing 0.5 photons on average, and observe short-time external efficiency of 25%, memory lifetime (1/*e*) of 86 ns, and below 10^{-4} added noise photons. Consequently, coupling this memory to a probabilistic source would enhance the on-demand photon generation probability by a factor of 12, the highest number yet reported for a noise-free, room temperature memory. This paves the way toward the controlled production of large quantum states of light from probabilistic photon sources.

INTRODUCTION

Large quantum states of light, where many photons occupy multiple modes in a coherent superposition of different configurations, are the backbone of photonic quantum communication, metrology, and computation (*1*). Optical photons are easily transmitted over complex networks and do not suffer from thermal noise at ambient temperature making photonic quantum information processing an appealing paradigm (*2*). However, the interaction between photons in common optical materials is extremely weak, leading to single-photon sources and two-photon gates that must rely on measurement and are therefore probabilistic. This renders the scaling-up of quantum photonic networks an exponentially hard problem.

Two approaches to this challenge are currently pursued. One approach focuses on developing new materials and systems for deterministic operation, such as single emitters strongly coupled to photonic structures (*3*–*6*) or cold ensembles of cooperative emitters (*7*). The second approach, which we follow here, focuses on actively synchronizing probabilistic elements in a repeat-until-success strategy (*2*, *8*). Here, every operation is repeated until it heralds a success, and its output is stored; when all operations are successful, their outputs are synchronously retrieved. This strategy requires memory modules that can efficiently store quantum states of light and retrieve them on demand, without additional noise (*9*, *10*). Many types of quantum optical memories have been demonstrated, motivated by the need for long-term storage in quantum repeaters (*9*, *11*) and for synchronizing high-bandwidth sources (*8*, *10*). None of these demonstrations, however, meets the combined requirements of high external efficiency, long lifetime, and low added noise.

Here, we demonstrate a fast ladder memory (FLAME) satisfying these requirements at ambient temperatures. FLAME uses a ladder-level scheme of electronic orbitals (in our case, the 5*s*, 5*p*, and 5*d* orbitals of warm rubidium atoms), as illustrated in Fig. 1A. A strong control pulse induces the coherent absorption of the signal pulse in the medium, thereby mapping the signal field onto the spatial field of quantum coherence between the lower and upper orbitals. A subsequent control pulse retrieves the signal via stimulated emission.

Department of Physics of Complex Systems, Weizmann Institute of Science, Rehovot 7610001, Israel.
*These authors contributed equally to this work.
†Corresponding author. Email: ofer.firstenberg@weizmann.ac.il

Very recently, Kaczmarek *et al.* (*12*) introduced the off-resonance cascaded absorption (ORCA) protocol, which is a far-detuned FLAME. They used cesium vapor to store and retrieve single photons from a heralded down-conversion source and demonstrated the preservation of nonclassical statistics. However, the large energy mismatch of the ladder levels in cesium limited the memory lifetime to a few nanoseconds. Here, we implement FLAME in rubidium, obtaining a memory lifetime much longer than in cesium while maintaining high bandwidth and low noise. We show that FLAME works both on resonance ($\Delta = 0$) and off resonance ($\Delta = 1.15$ GHz) with the intermediate ladder level. Despite the differences between these two regimes (*13*–*15*), we obtain high external efficiency in both.

The experimental arrangement is depicted in Fig. 1B. We prepare the ensemble by polarizing the atoms using circularly polarized (σ^+) optical pumping beams at 795 nm. To keep the polarized atoms within the maximally polarized subspace of the $5S_{1/2} - 5P_{3/2} - 5D_{5/2}$ ladder, we use σ^+ signal at 780 nm and σ^+ control at 776 nm (fig. S1). Transitions within this subspace are purely orbital, even when Δ and the control Rabi frequency Ω are not much larger than the hyperfine splitting.

Three main ingredients combine to explain the physics behind the success of FLAME. First, the fast time variation of the control field breaks the delay-bandwidth constraint of time-invariant linear resonant systems (*16*, *17*), thus enabling coherent absorption of signal pulses substantially shorter than the atomic resonance lifetime (*13*, *14*). Second, with entirely orbital transitions and no need for spin flips, the FLAME operation is essentially independent of hyperfine and fine interactions (*18*), making its bandwidth fundamentally limited only by the distance to adjacent orbitals. Third, the large Ω (and optionally large Δ) values diminish the effect of Doppler broadening and, by that, efficiently engage in the process all velocity groups of the thermal ensemble. This makes the resonant optical depth (OD) in our experiments (OD = 13) ideally as efficient as if the atoms were stationary (thus equivalent to $OD_{stat.} \approx 800$) and comparable to that of large ultracold ensembles (*19*, *20*). The OD and control intensity contribute equally to the storage efficiency for a given pulse duration (*13*), making their experimental availability the only practical limitation on the FLAME bandwidth.

Together with high bandwidth, a main appeal of FLAME over Λ-type (ground-state) memories is its immunity to four-wave mixing noise; in Λ-type configurations, the control may spontaneously Raman-scatter to form spurious spin waves, which are then retrieved as noise photons (*21*). This process is absent in a ladder configuration (*12*).

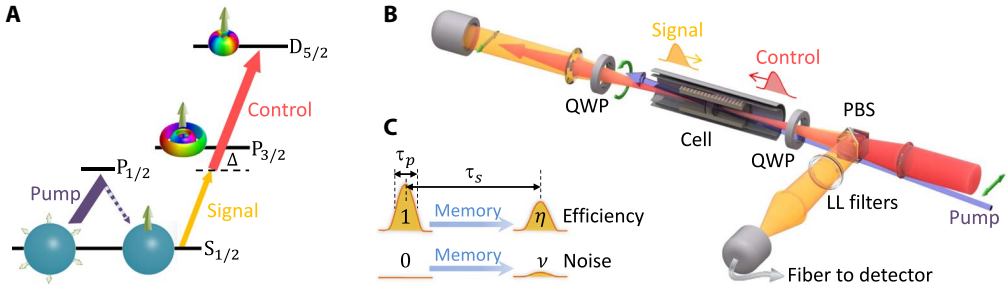

Fig. 1. FLAME scheme. (**A**) A ladder-level structure comprising purely orbital transitions (the surface colors display the phase structure of the orbitals 5*s*, 5*p*, and 5*d*) is achieved by optical pumping (purple) of the nuclear and electronic spins (green arrows) to the maximally polarized state. Nonzero detuning Δ from the intermediate level can be introduced. (**B**) To keep the ladder within the maximally polarized subspace, the counter-propagating signal and control beams are circularly polarized using quarter-wave plates (QWP; polarizations shown by green arrows). The collimated optical pump beams enter the cell at a small angular deviation. After storage and retrieval, a polarizing beam-splitter (PBS) picks out the signal. Scattered control light and spontaneous emission are filtered out spectrally by laser-line (LL) filters and spatially by a single-mode fiber coupled to the photodetector. (**C**) The parameters governing the synchronization capability of the memory are pulse duration τ_p, memory lifetime τ_s, retrieval efficiency η, and noise ν.

Furthermore, spurious excitations of the 5P and 5D levels are heavily suppressed by the frequency mismatch between the two ladder transitions and by the negligible excitation probability of the optical transition at room temperature.

In addition to reducing spurious excitations, the wavelength difference between the signal and control fields allows their separation by commercial interference filters. This enables high setup transmission so that the memory (external) efficiency approaches the (internal) efficiency of the storage process itself. However, the wavelength difference inevitably leads to a spatially varying phase of the stored coherence and thus to dephasing due to ballistic atomic motion. This dephasing, known as residual Doppler broadening, scales with the wave vector difference between the signal and control and is thus minimized in the counter-propagation geometry. In rubidium FLAME, the wave vector difference is ~ 0.5 % (coherence wavelength of ~ 150 μm), providing an excellent trade-off between the above competing factors. The resulting expected dephasing time is about 130 ns at the cell temperature of 100°C, comparable to the 240-ns radiative lifetime of the 5D level. Although this lifetime is shorter than that of most ground-state memories (*19*–*24*), it is much larger than the inverse bandwidth of FLAME, as required for efficient synchronization.

The memory parameters governing the synchronization performance are illustrated in Fig. 1C. For any storage time *t*, the external efficiency η_t is the ratio between the number of retrieved photons arriving at the detector and that of the incoming photons. The memory lifetime τ_s (defined by $\eta_{t=\tau_s} = \eta_0 e^{-1}$) and pulse duration τ_p determine the fractional delay τ_s/τ_p. The effective fractional delay $f_e = \eta_0\tau_s/\tau_p$ quantifies the synchronization capacity for an array of source-memory units (*8*). This is the enhancement factor, with respect to a bare source, of the probability that a single unit of such an array would generate a photon at the readout time.

Finally, the noise ν is the number of photons arriving at the detector absent an incoming signal. The noise-to-signal ratio $\mu_1 \equiv \nu/\eta_0$ quantifies the contamination of the retrieved state for one input photon (*25*).

RESULTS

The characterization of the memory lifetime and efficiency in the off-resonance case Δ = 1.15 GHz is shown in Fig. 2 (A to C). We store laser pulses with a duration of τ_p = 1.7 ns, containing 0.5 photons on average. These measurements are repeated on resonance (Δ = 0), with τ_p = 1.85 ns,

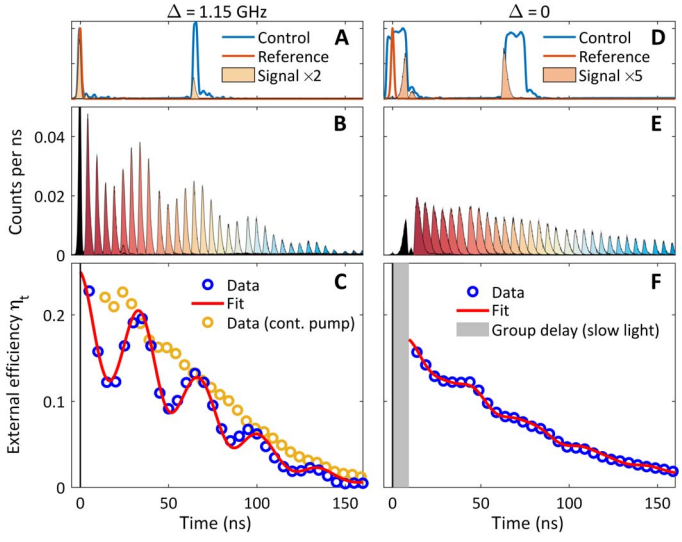

Fig. 2. FLAME operation for different storage times *t*, off resonance (left) and on resonance (right). (**A** and **D**) Typical pulse sequence, presented for *t* = 40 ns. The incoming pulse is shown for reference. (**B** and **E**) Traces from the single-photon counter for different storage times (colors). The blackened areas mark the portion of the leaked signal. (**C** and **F**) Decay of memory efficiency with *t*. Continuous optical pumping [yellow symbols in (C)] demonstrates the vanishing of beating for a fully polarized ensemble (while introducing more noise). Gray area in (F) marks the delay of the signal because of the reduced group velocity while the control pulse is on.

as shown in Fig. 2 (D to F). The pulse durations (and thus the demonstrated bandwidth of ~ 250 MHz) are limited by our driving electronics (see Materials and Methods). We adjust the timing and duration of the control pulses (see Fig. 2, A and D) for maximal storage efficiency. For the on-resonance case, we arrive at a long square control pulse, within which the signal exhibits a substantial group delay (≈ 9 ns), typical for storage via electromagnetically induced transparency (EIT) (*23*). In addition, the pulses retrieved on resonance are wider by ~ 60 % than the input pulse, compared to just ~ 10 % widening for off resonance.

We turn off the optical pumping 1.2 μs before the storage to reduce the fluorescence from excited atoms (see section S2). During the off time, unpolarized atoms enter the interaction region, reducing the average polarization and enabling the excitation of additional hyperfine

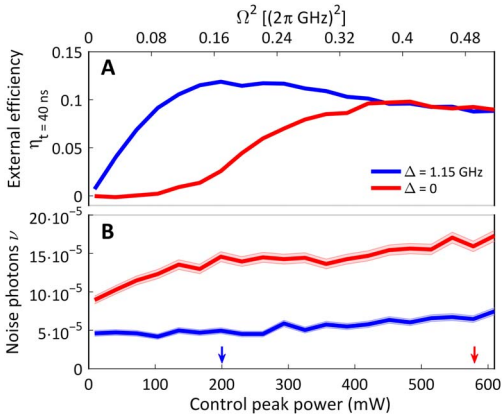

Fig. 3. Efficiency and noise dependence on control power (bottom axis) or control Rabi frequency Ω (top axis). (**A**) Memory efficiency for t = 40 ns. (**B**) Total photons in the collection window absent an incoming signal (shaded areas are 1σ statistical uncertainty). Note that the collection window is larger by 45% in the Δ = 0 case (for accommodating the wider retrieved signal). The arrows mark the operating powers of Fig. 2.

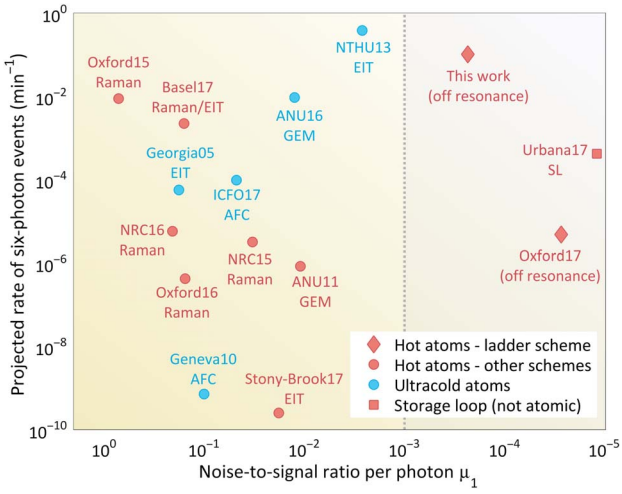

Fig. 4. Projected performance of reported quantum memories for synchronizing six heralded single-photon sources: High production rate and low noise (top-right quarter) are desired. The vertical dotted line marks the value 10^{-3} used as the success probability of the sources (thus indicating their intrinsic noise-to-signal ratio). The labels present the group, year, and memory protocol. AFC, full atomic frequency comb; EIT, EIT storage; GEM, gradient echo memory; Raman, far-detuned Raman storage; SL, storage loop. The calculation takes the source repetition rate as the minimum between τ_p^{-1} and 50 GHz, the latter estimating the current limit of the required feed-forward electronics. Source data, references, and additional details are provided in section S3.

sublevels in $5D_{5/2}$. The beats in Fig. 2C (also visible in Fig. 2F) are due to interference between the retrieval amplitudes from these sublevels. The beating visibility vanishes for continuous pumping (Fig. 2C, yellow) and conversely increases without optical pumping (see fig. S2).

We fit the measured efficiency to a simple model accounting for the beats (with the known hyperfine frequencies) and for inhomogeneous and homogeneous decays (see Materials and Methods). The dominant decay source is found to be motional dephasing. For Δ = 1.15 GHz, we extract from the fit the short-time efficiency $\eta_0 = 0.25\,(1)$ and lifetime τ_s = 86 (2) ns. This yields an effective fractional delay $f_e = \eta_0\tau_s/\tau_p = 12.6$, the largest yet reported for noise-free memories at ambient temperature. For Δ = 0, we extract $\eta_0 = 0.171$ (4) and $\tau_s = 82$ (1) ns, yielding $f_e = 7.6$.

The noise ν is measured by repeating the experiment with no input signal. We observe no dependence of the noise on storage time and find $\mu_1 = \nu/\eta_0 = 11\,(1) \times 10^{-4}$ for Δ = 0 and $\mu_1 = 2.3\,(3) \times 10^{-4}$ for Δ = 1.15 GHz, an order of magnitude lower than current ground-state memories.

The efficiency and noise as a function of control power are shown in Fig. 3 for a fixed storage time. The Δ = 0 case reaches the maximal efficiency at higher control power. The noise ν scales linearly with control power, affirming the absence of four-wave mixing, which would have yielded a quadratic dependence. We attribute the noise to unfiltered control photons and residual fluorescence due to the optical pumping (see section S2). These measurements, in combination with the direct verification by Kaczmarek *et al.* (*12*) that the memory preserves antibunching, establish the suitability of FLAME for quantum synchronization applications.

DISCUSSION

The differences between on- and off-resonance FLAME, evident in the optimal duration (Fig. 2, A and D) and power (Fig. 3A) of the control pulses, imply that the storage dynamics in the two regimes are somewhat distinct. It appears that off-resonance FLAME, or ORCA (*12*), performs slightly better. On the other hand, they exhibit comparable efficiencies at high control power, once the resonant absorption has been overcome in the Δ = 0 case. Group velocity dispersion moderately widens the pulse on resonance but is expected to vanish at higher control power (*15*); the off-resonance storage allows a greater degree of control over the retrieved pulse shape (*26*), and the observed minor widening can be circumvented by fine-tuning the shape of the control pulses. Future work could explore the optimal regime of operation for FLAME.

As a benchmark, we examine a test case of synchronizing six probabilistic single-photon sources having initial success probability of 10^{-3}, following Nunn *et al.* (*8*). Figure 4 summarizes the projected performance of reported memory protocols, demonstrating the FLAME advantage.

In conclusion, we have demonstrated FLAME in rubidium, both on and off resonance, and have shown that very low noise levels, high external efficiency, and high fractional delay are all simultaneously achievable at ambient temperature. There is much room for improvement of rubidium FLAME beyond our initial demonstration. Specifically, we estimate that the control power and ODs required for storage of 200-ps pulses with 50% external efficiency are within current experimental reach (see Materials and Methods). These parameters could enable the synchronization of, for example, 10 probabilistic single-photon sources in less than 1 s, paving the way to quantum information processing with large quantum states of light. Furthermore, by coupling it to strongly interacting Rydberg states (*27*), FLAME can potentially be used for building deterministic quantum gates or sources.

MATERIALS AND METHODS

Experimental design

A detailed scheme of the experimental setup is presented in Fig. 5. The core of the setup comprises a 780-nm distributed Bragg reflector (DBR) diode laser, serving as the signal beam, and a 776-nm external cavity diode laser (ECDL) amplified by a tapered amplifier (TA), serving as

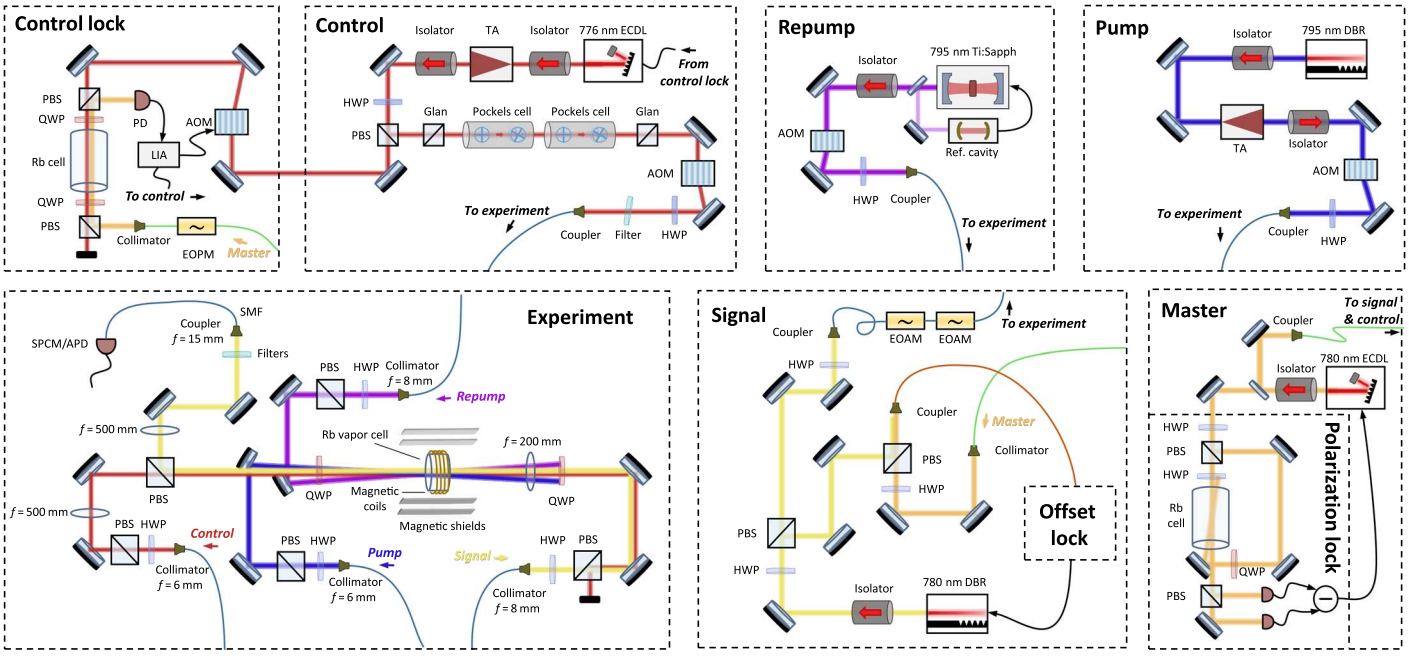

Fig. 5. Experimental setup. EOAM, electro-optic amplitude modulator; EOPM, electro-optic phase modulator; Glan, Glan-laser polarizer; HWP, half-wave plate; LIA, lock-in amplifier; PD, photodetector; SPCM, single-photon counting module.

the control beam. The signal laser was offset-locked to a master ECDL using a fast beat note detector, whereas the master laser was polarization-locked to a reference ^{85}Rb cell. The control laser and the master laser, modulated by a fiber electro-optic phase modulator, counter-propagated through a ^{87}Rb reference cell, and the control laser was locked to the two-photon absorption or transparency feature. In this configuration, the frequencies of the signal and control can be independently tuned, while being locked to the master laser, whereas their sum—and thus the two-photon detuning—is insensitive to slow frequency drifts of the master laser.

The signal field was amplitude-modulated in time by two fiber electro-optic amplitude modulators to carve a Gaussian pulse of 1.7-ns full width at half maximum (FWHM) (for the off-resonance measurements) or 1.85-ns FWHM (for the on-resonance measurements), with a combined extinction ratio of 1:3000. The control field was amplitude-modulated by two Pockels cells (PCs), followed by an acousto-optic modulator (AOM), to create two pulses of 2.5-ns FWHM (for the off-resonance measurements) or 10-ns FWHM (for the on-resonance measurements), with a combined extinction ratio of 1:10,000 outside the two pulses, and of between 1:200 and 1:10,000 between the pulses, depending on the storage time (due to the 20-ns switching time of the AOM). The repetition rate of the experiment was set by that of the PCs to 100 kHz.

After the modulators, the control beam was passed through a tilted 780-nm bandpass filter (Semrock LL01-780-12.5) functioning as a 776-nm bandpass filter, filtering out other frequencies that might be produced in the TA. The signal and control pulses were passed through single-mode fibers (SMFs), aligned with each other in a counter-propagating geometry, and overlapped at the center the vapor cell. The signal (control) beam was focused down to $2w_0$ = 170 μm (410 μm) waist diameter ($1/e^2$). Both beams were σ^+ polarized. The control peak power used in the measurements shown in Fig. 2 for off (on) resonance is 200 mW (580 mW), with a corresponding peak Rabi frequency of $2\pi \times$ 410 MHz ($2\pi \times$ 700 MHz).

The 10-mm-long ^{87}Rb vapor cell was anti-reflection–coated. It was heated to 72°C at its coldest spot and 100°C at the hottest spot using two electrical current heaters to set a Rb density of 6.5×10^{11} cm^{-3} and an OD ≈ 9. We obtained OD ≈ 15 with continuous optical pumping and OD ≈ 13 (during the storage) when the optical pumping was turned off for storage.

After the cell, the signal beam was passed through a PBS and two 780-nm bandpass filters (at normal incidence) to filter out any residual 776-nm and 795-nm components. It was then coupled to an SMF acting as a spatial filter, removing most of the spatially incoherent fluorescence emitted from the cell at 780 nm. The SMF was coupled either to a fast linear avalanche photodetector (APD) with a bandwidth of 1 GHz or to a SPCM connected to a time tagger with time bins of 100 ps.

Two optical pumping beams, a "pump" and a "repump," were introduced into the system for a duration of 8.2 μs out of the 10-μs period of the experimental cycle. These beams were both at 795 nm, σ^+ polarized, and separated one from the other by 6.8 GHz such that the pump (repump) was resonant with the $F = 2 \rightarrow F' = 2$ ($F = 1 \rightarrow F' = 2$) transitions of the rubidium D1 line. The pump beam originated from a temperature- and current-stabilized DBR diode laser amplified by a TA, and the repump beam originated from a continuous-wave Ti:sapphire laser. The pump beam power at the vapor cell was 100 mW, and that of the repump beam was 250 mW. The pump beam was 1.2 mm wide, and the repump beam was 1.6 mm wide. They were directed at small angles with respect to the control beam. To minimize the noise due to collisional fluorescence from atoms excited by the optical pumping (see section S2), the experiment was performed 1.2 μs after the optical pumping beams have been switched off by AOMs. A ~1 G magnetic field applied along the optical axis and a two-layer μ-metal magnetic shield protected the spin polarization from dephasing and thus from depumping due to ambient magnetic fields.

For the storage experiments presented in Fig. 2 and fig. S2, each data point was collected over 1 million experimental cycles using the SPCM.

For the noise measurements presented in Fig. 3B, each data point was collected over 5 million cycles using the SPCM. The measurement of efficiency versus control power in Fig. 3A was collected using the fast APD and with weak laser pulses.

Analysis of memory efficiency

The external efficiency is defined as the product of the internal efficiency and the setup transmission. The internal efficiency is calculated as the ratio of the area of the retrieved pulse to that of the signal pulse transmitted through the system without the control beams (at a detuning of 1.15 GHz, where its absorption is $< 10^{-3}$). The area was summed over an integration window of 5.5 ns (8 ns) for off-resonance (on-resonance) operation, containing the entire retrieved pulse.

The setup transmission was measured as the ratio of the input signal intensity just before the vapor cell, and the signal intensity reaching the detector after passing through the entire system, including the bandpass filters and the SMF. The total setup transmission in our system was measured to be $T_{\mathrm{setup}} = 78.0(5)$ %, with the filters transmitting 97 %, the SMF coupling and transmission being 90.0(4) %, and the rest of the system (vapor cell and other optics) transmitting 89.0(4)%.

The decay of coherence during storage stems from both homogeneous and inhomogeneous processes, represented by the decay times τ_σ and τ_γ, respectively. The envelope decay is described by $\eta_0 e^{-(t-t_0)/\tau_\gamma} e^{-(t-t_0)^2/(2\tau_\sigma^2)}$, where $\eta_0 = \eta(t_0)$ is the short-time external storage efficiency. We identified the $1/e$ memory lifetime τ_s and a complementary parameter $\bar{\tau}$ by the relations $\tau_\gamma = \tau_s\bar{\tau}/(\bar{\tau} - \tau_s)$ and $\tau_\sigma = \sqrt{\tau_s\bar{\tau}/2}$. The solid lines in Fig. 2 (C and F) are fits to the data using the model

$$\eta(t) = \eta_0 e^{-\left[\frac{1}{\tau_s\bar{\tau}}(t-t_0-\tau_s)(t-t_0+\bar{\tau})+1\right]} \left| \frac{1 + Ae^{-i\omega_{43}(t-t_0)} + Be^{-i\omega_{42}(t-t_0)}}{1+A+B} \right|^2 \quad (1)$$

where the hyperfine frequency differences within the $5D_{5/2}$ level are taken to be $\omega_{43} = 2\pi \times 28.82$ MHz, and $\omega_{42} = 2\pi \times 51.77$ MHz (*28*). The $5D_{5/2}$ $F = 1$ level is neglected in this model.

Because the stored pulse duration was much shorter than the inverse of the frequency differences within the $5D_{5/2}$ level, the stored coherences of different hyperfine states were all in-phase at the time of storage, t_0. We were thus able to find t_0, which might be offset from the peak of the signal reference because of the modified group velocity on and off resonance, by fitting Eq. 1 to the measured oscillations. The obtained fit parameters are summarized in Table 1. The lifetime is governed by the inhomogeneous (motional) dephasing $\tau_\sigma = \sqrt{\tau_s\bar{\tau}/2}$, and we can extract from the fit $\tau_\sigma = 65(4)$ ns for the off-resonance case and $\tau_\sigma = 117(7)$ for the on-resonance case. The much longer homogeneous decay time cannot be faithfully determined from the data.

Table 1. Memory parameters extracted from the measurements using the fit function of Eq. 1. Uncertainties in parentheses are 1σ SD.

	τ_s (ns)	η_0 (%)	$\bar{\tau}$ (ns)	t_0 (ns)	A	B
Off-resonance	86(2)	25.1(8)	101(12)	−1.0(3)	0.160(9)	0.006(9)
On-resonance	82(1)	17.1(3)	337(43)	9.2(6)	0.032(4)	0.007(4)

The main contribution to the storage decay rate is due to ballistic thermal motion of the hot atoms. This includes both the longitudinal residual Doppler broadening $\Delta k v_T = 1.22\,(2\pi)$ MHz and the transversal "time-of-flight" rate of the atoms leaving the beam $v_T/w_0 = 0.34\,(2\pi)$ MHz, where w_0 is the signal beam waist radius. The corresponding inhomogeneous decay time is 102 ns. Summing these rates with the homogeneous "natural" coherence decay rate 0.33 (2π) MHz of the $5D_{5/2}$ level, the storage lifetime was estimated to be 84 ns, consistent with the above results. We believe that the lower inhomogeneous lifetime τ_σ for the off-resonance case is related to its high bandwidth, addressing most atoms including those with high thermal velocity. Understanding the details of this dephasing mechanism in the context of the differences between the on- and off-resonance cases will be part of future work.

In accordance with the above values, the short-time internal efficiency for $\Delta = 1.15$ GHz is $\eta_0^{\mathrm{int}} = 32(1)\%$, and for $\Delta = 0$, it is $\eta_0^{\mathrm{int}} = 22.0(4)\%$. For the off-resonance regime, we can roughly estimate the expected storage efficiency using the formalism developed by Nunn *et al.* (*29*). We used $\gamma \times \mathrm{OD}_{\mathrm{stat.}} = 5\,(2\pi)$ GHz [where $\gamma = 6\,(2\pi)$ MHz is the spectral width of the intermediate level and $\mathrm{OD}_{\mathrm{stat.}}$ is the OD had the atoms were stationary] and $\Omega/\Delta = 0.36$ to calculate for a pulse width $\tau_p = 1.7$ ns the so-called coupling parameter $\mathcal{C} = (\Omega/\Delta)\sqrt{\tau_p \gamma \mathrm{OD}_{\mathrm{stat.}}}/4 = 0.66$. The resulting (internal) efficiency is $\eta_0^{\mathrm{int}}(\mathcal{C}) \approx 16\%$ (*29*), which is lower but qualitatively agrees with the measured value. The same formalism implies that, for control intensity and OD an order of magnitude larger than those available in our current setup, storage of 200-ps pulses with 50 % efficiency ($\mathcal{C} \approx 1$) is possible. This estimation assumes a control power of 6 W (30 times larger than the 200 mW used for the above calculation so that $\Omega \rightarrow \sqrt{30}\Omega$) readily available with current laser technology such as continuous Ti:sapphire lasers, larger detuning ($\Delta \rightarrow 3\Delta$) for avoiding resonant absorption of the broadband pulses, and a density 10 times larger ($\mathrm{OD}_{\mathrm{stat.}} \rightarrow 10 \times \mathrm{OD}_{\mathrm{stat.}}$), readily achievable by heating the cell to 105°C.

SUPPLEMENTARY MATERIALS

Supplementary material for this article is available at http://advances.sciencemag.org/cgi/content/full/4/1/eaap8598/DC1

section S1. Atomic level scheme
section S2. Noise sources
section S3. Source data and performance analysis of different quantum optical memories
fig. S1. Rubidium level scheme.
fig. S2. External efficiency as a function of storage time *t*, with the optical pumping continuously on (yellow) or switched off before storage (red), or with no pumping at all (blue).
table S1. Memory parameters used for compiling Fig. 4.
table S2. Memory parameters used for compiling Fig. 4 (cont.).
References (*30*–*44*)

REFERENCES AND NOTES

1. J. L. O'Brien, Optical quantum computing. *Science* **318**, 1567–1570 (2007).
2. E. Knill, R. Laflamme, G. J. Milburn, A scheme for efficient quantum computation with linear optics. *Nature* **409**, 46–52 (2001).
3. X. Ding, Y. He, Z.-C. Duan, N. Gregersen, M.-C. Chen, S. Unsleber, S. Maier, C. Schneider, M. Kamp, S. Höfling, C.-Y. Lu, J.-W. Pan, On-demand single photons with high extraction efficiency and near-unity indistinguishability from a resonantly driven quantum dot in a micropillar. *Phys. Rev. Lett.* **116**, 020401 (2016).
4. I. Shomroni, S. Rosenblum, Y. Lovsky, O. Bechler, G. Guendelman, B. Dayan, All-optical routing of single photons by a one-atom switch controlled by a single photon. *Science* **345**, 903–906 (2014).
5. B. Hacker, S. Welte, G. Rempe, S. Ritter, A photon-photon quantum gate based on a single atom in an optical resonator. *Nature* **536**, 193–196 (2016).
6. A. Sipahigil, R. E. Evans, D. D. Sukachev, M. J. Burek, J. Borregaard, M. K. Bhaskar, C. T. Nguyen, J. L. Pacheco, H. A. Atikian, C. Meuwly, R. M. Camacho, F. Jelezko, E. Bielejec,

H. Park, M. Ločar, M. D. Lukin, An integrated diamond nanophotonics platform for quantum-optical networks. *Science* **354**, 847–850 (2016).
7. O. Firstenberg, T. Peyronel, Q.-Y. Liang, A. V. Gorshkov, M. D. Lukin, V. Vuletić, Attractive photons in a quantum nonlinear medium. *Nature* **502**, 71–75 (2013).
8. J. Nunn, N. K. Langford, W. S. Kolthammer, T. F. M. Champion, M. R. Sprague, P. S. Michelberger, X.-M. Jin, D. G. England, I. A. Walmsley, Enhancing multiphoton rates with quantum memories. *Phys. Rev. Lett.* **110**, 133601 (2013).
9. C. Simon, M. Afzelius, J. Appel, A. Boyer de La Giroday, S. J. Dewhurst, N. Gisin, C. Y. Hu, F. Jelezko, S. Kröll, J. H. Müller, J. Nunn, E. S. Polzik, J. G. Rarity, H. D. Riedmatten, W. Rosenfeld, A. J. Shields, N. Sköld, R. M. Stevenson, R. Thew, I. A. Walmsley, M. C. Weber, H. Weinfurter, J. Wrachtrup, R. J. Young, Quantum memories. *Eur. Phys. J. D* **58**, 1–22 (2010).
10. K. Heshami, D. G. England, P. C. Humphreys, P. J. Bustard, V. M. Acosta, J. Nunn, B. J. Sussman, Quantum memories: Emerging applications and recent advances. *J. Mod. Opt.* **63**, 2005–2028 (2015).
11. N. Sangouard, C. Simon, H. de Riedmatten, N. Gisin, Quantum repeaters based on atomic ensembles and linear optics. *Rev. Mod. Phys.* **83**, 33–80 (2011).
12. K. T. Kaczmarek, P. M. Ledingham, B. Brecht, S. E. Thomas, G. S. Thekkadath, O. Lazo-Arjona, J. H. D. Munns, E. Poem, A. Feizpour, D. J. Saunders, J. Nunn, I. A. Walmsley, A high-speed noise-free optical quantum memory. http://arxiv.org/abs/1704.00013 (2017).
13. J. Nunn, I. A. Walmsley, M. G. Raymer, K. Surmacz, F. C. Waldermann, Z. Wang, D. Jaksch, Mapping broadband single-photon wave packets into an atomic memory. *Phys. Rev. A* **75**, 011401 (2007).
14. T. Golubeva, Y. M. Golubev, O. Mishina, A. Bramati, J. Laurat, E. Giacobino, High speed spatially multimode Λ-type atomic memory with arbitrary frequency detuning. *Eur. Phys. J. D* **66**, 275 (2012).
15. I. Novikova, A. V. Gorshkov, D. F. Phillips, A. S. Srensen, M. D. Lukin, R. L. Walsworth, Optimal control of light pulse storage and retrieval. *Phys. Rev. Lett.* **98**, 243602 (2007).
16. Q. Xu, P. Dong, M. Lipson, Breaking the delay-bandwidth limit in a photonic structure. *Nat. Phys.* **3**, 406–410 (2007).
17. K. L. Tsakmakidis, L. Shen, S. A. Schulz, X. Zheng, J. Upham, X. Deng, H. Altug, A. F. Vakakis, R. W. Boyd, Breaking Lorentz reciprocity to overcome the time-bandwidth limit in physics and engineering. *Science* **356**, 1260–1264 (2017).
18. E. Poem, C. Weinzetl, J. Klatzow, K. T. Kaczmarek, J. H. D. Munns, T. F. M. Champion, D. J. Saunders, J. Nunn, I. A. Walmsley, Broadband noise-free optical quantum memory with neutral nitrogen-vacancy centers in diamond. *Phys. Rev. B* **91**, 205108 (2015).
19. Y.-H. Chen, M.-J. Lee, I.-C. Wang, S. Du, Y.-F. Chen, Y.-C. Chen, I. A. Yu, Coherent optical memory with high storage efficiency and large fractional delay. *Phys. Rev. Lett.* **110**, 083601 (2013).
20. Y.-W. Cho, G. T. Campbell, J. L. Everett, J. Bernu, D. B. Higginbottom, M. T. Cao, J. Geng, N. P. Robins, P. K. Lam, B. C. Buchler, Highly efficient optical quantum memory with long coherence time in cold atoms. *Optica* **3**, 100 (2016).
21. P. S. Michelberger, T. F. M. Champion, M. R. Sprague, K. T. Kaczmarek, M. Barbieri, X. M. Jin, D. G. England,W. S. Kolthammer, D. J. Saunders, J. Nunn, I. A. Walmsley, Interfacing GHz-bandwidth heralded single photons with a warm vapour Raman memory. *New J. Phys.* **17**, 043006 (2015).
22. T. Chanelire, D. N. Matsukevich, S. D. Jenkins, S.-Y. Lan, T. A. B. Kennedy, A. Kuzmich, Storage and retrieval of single photons transmitted between remote quantum memories. *Nature* **438**, 833–836 (2005).
23. M. D. Eisaman, A. André, F. Massou, M. Fleischhauer, A. S. Zibrov, M. D. Lukin, Electromagnetically induced transparency with tunable single-photon pulses. *Nature* **438**, 837–441 (2005).
24. J. J. Longdell, E. Fraval, M. J. Sellars, N. B. Manson, Stopped light with storage times greater than one second using electromagnetically induced transparency in a solid. *Phys. Rev. Lett.* **95**, 063601 (2005).
25. D. J. Saunders, J. H. D. Munns, T. F. M. Champion, C. Qiu, K. T. Kaczmarek, E. Poem, P. M. Ledingham, I. A. Walmsley, J. Nunn, Cavity-enhanced room-temperature broadband Raman memory. *Phys. Rev. Lett.* **116**, 090501 (2016).
26. K. A. G. Fisher, D. G. England, J.-P. W. MacLean, P. J. Bustard, K. J. Resch, B. J. Sussman, Frequency and bandwidth conversion of single photons in a room-temperature diamond quantum memory. *Nat. Commun.* **7**, 11200 (2016).
27. F. Ripka, Y.-H. Chen, R. Löw, T. Pfau, Rydberg polaritons in a thermal vapor. *Phys. Rev. A* **93**, 053429 (2016).
28. F. Nez, F. Biraben, R. Felder, Y. Millerioux, Optical frequency determination of the hyperfine components of the 5S12-5D32 two-photon transitions in rubidium. *Opt. Commun.* **102**, 432–438 (1993).
29. J. Nunn, "Quantum memory in atomic ensembles," thesis, University of Oxford, Oxford, UK (2008), chap. 5.
30. M. D. Rotondaro, G. P. Perram, Role of rotational-energy defect in collisional transfer between the $5^2 P_{1/2,3/2}$ levels in rubidium. *Phys. Rev. A* **57**, 4045–4048 (1998).
31. H. de Riedmatten, M. Afzelius, M. U. Staudt, C. Simon, N. Gisin, A solid-state light-matter interface at the single-photon level. *Nature* **456**, 773–777 (2008).
32. E. Saglamyurek, M. G. Puigibert, Q. Zhou, L. Giner, F. Marsili, V. B. Verma, S. W. Nam, L. Oesterling, D. Nippa, D. Oblak, W. Tittel, A multiplexed light-matter interface for fibre-based quantum networks. *Nat. Commun.* **7**, 11202 (2016).
33. L.-M. Duan, M. D. Lukin, J. I. Cirac, P. Zoller, Long-distance quantum communication with atomic ensembles and linear optics. *Nature* **414**, 413–418 (2001).
34. K. Makino, Y. E. Hashimoto, J. Yoshikawa, H. Ohdan, T. Toyama, P. van Loock, A. Furusawa, Synchronization of optical photons for quantum information processing. *Sci. Adv.* **2**, e1501772 (2016).
35. J.-P. Dou, A.-l. Yang, M.-Y. Du, D. Lao, J. Gao, L.-F. Qiao, H. Li, X.-L. Pang, Z. Feng, H. Tang, X.-M. Jin, A broadband DLCZ quantum memory in room-temperature atoms. http://arxiv.org/abs/1704.06309 (2017).
36. D. G. England, K. A. G. Fisher, J.-P. W. MacLean, P. J. Bustard, R. Lausten, K. J. Resch, B. J. Sussman, Storage and retrieval of THz-bandwidth single photons using a room-temperature diamond quantum memory. *Phys. Rev. Lett.* **114**, 053602 (2015).
37. P. J. Bustard, D. G. England, K. Heshami, C. Kupchak, B. J. Sussman, Reducing noise in a Raman quantum memory. *Opt. Lett.* **41**, 5055–5058 (2016).
38. J. Wolters, G. Buser, A. Horsley, L. Béguin, A. Jöckel, J.-P. Jahn, R. J. Warburton, P. Treutlein, Simple atomic quantum memory suitable for semiconductor quantum dot single photons. *Phys. Rev. Lett.* **119**, 060502 (2017).
39. M. Namazi, C. Kupchak, B. Jordaan, R. Shahrokhshahi, E. Figueroa, Ultralow-noise room-temperature quantum memory for polarization qubits. *Phys. Rev. Appl.* **8**, 034023 (2017).
40. M. Hosseini, B. M. Sparkes, G. Campbell, P. K. Lam, B. C. Buchler, High efficiency coherent optical memory with warm rubidium vapour. *Nat. Commun.* **2**, 174 (2011).
41. M. Hosseini, G. Campbell, B. M. Sparkes, P. K. Lam, B. C. Buchler, Unconditional room-temperature quantum memory. *Nat. Phys.* **7**, 794–798 (2011).
42. M. Afzelius, I. Usmani, A. Amari, B. Lauritzen, A. Walther, C. Simon, N. Sangouard, J. Minář, H. de Riedmatten, N. Gisin, S. Kröll, Demonstration of atomic frequency comb memory for light with spin-wave storage. *Phys. Rev. Lett.* **104**, 040503 (2010).
43. A. Seri, A. Lenhard, D. Rielnder, M. Gündoğan, P. M. Ledingham, M. Mazzera, H. de Riedmatten, Quantum correlations between single telecom photons and a multimode on-demand solid-state quantum memory. *Phys. Rev. X* **7**, 021028 (2017).
44. F. Kaneda, F. Xu, J. Chapman, P. G. Kwiat, Quantum-memory-assisted multi-photon generation for efficient quantum information processing. *Optica* **4**, 1034–1037 (2017).

Acknowledgments: We thank J. Nunn for stimulating discussions. **Funding:** We acknowledge financial support by the Israel Science Foundation and Israeli Centers of Research Excellence, European Research Council starting investigator grant Q-PHOTONICS 678674, the Minerva Foundation, the Sir Charles Clore Research Prize, and the Laboratory in Memory of Leon and Blacky Broder. **Author contributions:** All authors contributed to the experimental design, construction, data collection, and analysis of this experiment. R.F. claims responsibility for Figs. 1 to 3 and figs. S1 and S2; E.P. and O.F. produced Fig. 4 and its data; and O.L. produced Fig. 5. The authors wrote the manuscript together. **Competing interests:** E.P. is an inventor on a PCT patent application related to this work (PCT application no. PCT/GB2017/050892, filed 30 March 2017). All other authors declare that they have no competing interests. **Data and materials availability:** All data needed to evaluate the conclusions in the paper are present in the paper and/or the Supplementary Materials. The data used in this work are also available online at http://www.weizmann.ac.il/complex/Firstenberg/data011. Additional data related to this paper may be requested from the authors.

Submitted 3 September 2017
Accepted 8 December 2017
Published 12 January 2018
10.1126/sciadv.aap8598

Citation: R. Finkelstein, E. Poem, O. Michel, O. Lahad, O. Firstenberg, Fast, noise-free memory for photon synchronization at room temperature. *Sci. Adv.* **4**, eaap8598 (2018).

Fast, noise-free memory for photon synchronization at room temperature

Ran Finkelstein, Eilon Poem, Ohad Michel, Ohr Lahad and Ofer Firstenberg

Sci Adv **4** (1), eaap8598.
DOI: 10.1126/sciadv.aap8598